Highly stable and active catalyst for hydrogen production from biogas

A. Serrano-Lotina*, L. Daza

Instituto de Catálisis y Petroleoquímica (CSIC), C/Marie Curie 2 L10, Campus Cantoblanco, 28049 Madrid, Spain

HIGHLIGHTS

- We used a La-promoted catalyst obtained from a hydrotalcite precursor.
- The catalyst was tested for dry reforming of methane to syngas during 300 h.
- No sign of deactivation was detected, although carbon deposited.
- The deposited carbon consists of carbon nanotubes and nanofibres with defects in their structure.

ARTICLE INFO

ABSTRACT

A La-NiMgAlO catalyst, obtained after calcination of a hydrotalcite precursor, was evaluated in dry reforming of methane. The catalyst showed no sign of deactivation during a 300 h test. CH_4 and CO_2 conversion were higher than thermodynamic equilibrium estimation which suggests the participation of other reactions.

Used catalyst was characterized by several techniques (TPO, XPS and Raman spectroscopy and SEM and TEM microscopy) in order to establish whether carbon was deposited and its nature. Two different types of carbon were present: carbon nanotubes (CNTs) and carbon nanofibres (CNFs). These filamentous carbons were well-crystallize but with many structural defects, which can increase the resistivity to fracture and therefore prevent the encapsulation of active sites. In addition, graphite can act as a CH_x collector, limiting the deactivation process. The small Ni particles diameter, together with its broad distribution, seems to have also a beneficial effect on the catalytic performance.

1. Introduction

There is a growing interest in the development of power sources that use renewable fuels and reduce emission of pollutants. This interest is justified by the heightening concern about environmental degradation, energy security as well as the possible exhaustion of the fossil fuel resources. One alternative is to use the biogas generated from sewage or wastewater anaerobic digestion. The high levels of CO_2 (25–45%) and CH_4 (55–75%) enable the conversion of biogas to synthesis gas (CO + H_2) by dry reforming ($CH_4 + CO_2 \leftrightarrows 2H_2 + 2CO$).

Dry reforming process becomes advantageous compared to steam reforming since (i) H_2/CO product ratio is near one, which is suitable for further use in the production of oxygenated compounds as well as for Fischer–Tropsch synthesis for the production of liquid hydrocarbons [1]; (ii) the separation of CO_2, which is an energy intensive and a rather costly process, is not necessary [2].

Nevertheless, the major drawback of dry reforming of methane is deactivation of the catalysts, mainly caused by deposition of inactive carbon, sintering and catalyst poison [3]. Since biogas contains between 0.1 and 0.5% of H_2S and small amounts of other sulphur compounds such as methanethiol (MeSH) and dimethyl sulphide (DMS), a previous desulfurization step is necessary to avoid the deactivation produced by the chemisorption of sulphur on metal catalyst [4].

In order to minimize coke formation two approaches can be taken into account. The first one can be executed by working at high temperatures, low space velocities or diluting reaction mixture [5,6]. Other alternative is controlling the reaction kinetically by using appropriate catalysts and supports. Considering the final application, the second alternative is the most appropriate since it will lower the operation costs. Therefore, many efforts are focused on the development of catalysts which exhibited high activities as well as good stabilities under reaction conditions.

The most active catalysts in dry reforming of methane are metal transition of the VIII-B group (Rh, Pt, Ru, Ir and Ni) [7–10]. Noble metal catalysts show the best performance [11], but the high cost

---

* Corresponding author. Tel.: +34 91 5854793; fax: +34 91 5854760.
E-mail address: asl@icp.csic.es (A. Serrano-Lotina).

and low availability make their use unviable. In order to improve the catalytic performance and minimize coking of the Ni based catalyst, several parameters can be modified, such as the kind of support, the metal content, the preparation method or the addition of promoters into the catalyst formulation [12–14]. In this context, hydrotalcites have been studied as precursors which after calcination lead to catalysts which show good performances in dry reforming of methane [15]. These catalysts show high dispersion as well as high surface area and basic properties which improved CO_2 chemisorption and consequently the resistance to coke formation [16]. Previous works [17] reported a great enhance of the stability when lanthanum is added. It strengthens CO_2 adsorption on the support and it also favour metal dispersion and the formation of a dynamic oxygen pool which favours coke removal [18,19]. Previous studies showed that the most appropriate Mg/Al molar ratio and calcination temperature are 2.3 and 750 °C, respectively [20–22].

There are only a few publications dealing with long-term stability of catalysts used in dry reforming of methane and almost all of them [23–25] were performed at high operating temperatures ($T > 750$ °C) which disfavour carbon deposition and therefore catalyst deactivation. Xu et al. [23] reported a great stability during 290 h operating at 800 °C, CH_4:CO_2 ratio of 1:1 and at 6000 cm^3 g_{cat}^{-1} h^{-1}. CH_4 and CO_2 conversions were stable at 93.7 and 94.0%, respectively, while H_2/CO ratio stayed at 0.97. They also reported a low average coking rate: 0.0946 mg g_{cat}^{-1} h^{-1}. Kang et al. [24] evaluated their catalyst during 150 h, working at 800 °C, CH_4:CO_2:N_2 ratio of 1:1:1 and at 30 cm^3 g_{cat}^{-1} h^{-1}. CH_4 and CO_2 conversions were stable at 92 and 95%, respectively while H_2/CO ratio stayed at 0.95. The average coking rate of this catalyst was 20.5 mg g_{cat}^{-1} h^{-1}. Al-Fatesh et al. [25] detected small changes in CH_4 and CO_2 conversions when they operated their catalyst at 850 °C, CH_4:CO_2:N_2 ratio of 5:5:1 and at 2640 cm^3 g_{cat}^{-1} h^{-1} during 130 h. The conversions evolved from 91.0 to 87.6% for CH_4 and from 98.3 to 91.0 for CO_2. However, they reported a very slow average coking rate (0.12 mg g_{cat}^{-1} h^{-1}). H_2/CO ratio remained constant at 0.99. Zhang et al. [26] reported a great stability over a Ni–Co bimetallic catalyst which was stable during the 250 h test, when it was tested at 750 °C, CH_4:CO_2:N_2 ratio of 1:1:1 and at 180,000 cm^3 g_{cat}^{-1} h^{-1} (differential conditions). They did not detect carbon deposits. These last two authors operate diluting the feeding which minimizes coke formation.

Consequently, the aim of this work was to study the stability of the catalyst in a long term experiment, performed at lower temperatures than the usually reported, as well as to evaluate and characterize carbon deposition.

2. Experimental

2.1. Catalyst preparation

The catalyst was obtained after calcination at 750 °C of a hydrotalcite precursor, which was prepared by co-precipitation, according to a previously reported method [17,21]. The final measured Mg/Al molar ratio was 2.3 whereas Ni and La contents were 2.8 and 1.9%, respectively.

2.2. Catalytic tests

Catalytic test was carried out in a Microactivity Reference PID Eng&Tech equipment, in a tubular fixed-bed stainless steel (Ni free) reactor at 750 °C, a CH_4:CO_2 molar ratio of 1:1 and GHSV of 4800 cm^3 g_{cat}^{-1} h^{-1}. This is the highest space velocity necessary to achieve the maximum conversion. Therefore, deactivation would not be hidden as a consequence of an excess of active sites. Excessive pressure drop was avoided by choosing a catalyst particle

size between 0.5 and 0.42 mm. A more detailed description of the testing protocol can be found elsewhere [17]. Reaction products were analysed with an Agilent chromatograph 6890N connected in line, equipped with a TCD detector and Chromosob 102 and Porapak P5 Q columns. Commercial CH_4 (99.5%), N_2, H_2, and CO_2 (99.999%), from Praxair, served as reactants.

In order to only reduce the segregated NiO, the catalyst was pretreated in situ at 650 °C with pure hydrogen during 1 h [20].

2.3. Characterization after test

Temperature programmed oxidation (TPO-MS) of tested catalyst was conducted in a Mettler-Toledo TGA/SDTA 851 thermo-balance with STAR 8.10 software coupled to a mass spectrometer detector Pfeiffer Thermostar GSD 301 T3. It was performed between 25 and 900 °C (5 °C min^{-1}) using a mixture of O_2/N_2 10/40 mLN min^{-1}. Carbon gasification was monitored by CO_2^+ signal ($m/z = 44$). X-ray photoelectron spectroscopy spectra were recorded using a spectrometer with a UHV system (pressure: 10^{-10}–10^{-9} mbar), a PHOIBOS 150 9MCD analyzer and a Multi-Channeltron detector. The used excitation source was Mg Kα radiation ($hν = 1253.6$ eV; 200 W; 12 kV; pass energy = 25 eV). Shirley-type background was subtracted from recorded signals. The spectra were fitted using Gauss–Lorentz curves. Raman spectra were collected in a Renishaw System 1000 spectrometer equipped with Ar ion laser (Spectra Physics, $λ = 514$ nm, power 19 mW, 1 mW on sample), a cooled CCD detector (-73 °C) and a holographic super-Notch filter to remove the elastic scattering. The spectral resolution was ca. 3 cm^{-1} and spectrum acquisition consisted of 10 accumulations of 30 s. The spectra were recorded at ambient temperature. SEM facility comprises a Hitachi S-3000N Scanning Electron Microscope coupled to an INCAx-sight energy-dispersive spectrometer, using a Sputter Coater SC502 to pre-treat the samples. TEM characterization was carried out in a JEOL Model JEM-1200 EXII transmission electron microscope equipped with an emission source of electron at 200 kV. Samples were ultrasonically dispersed in ethanol and a few drops were placed on a holey-carbon-coated copper grid, allowing the solvent to evaporate in air before TEM observation.

3. Results and discussion

3.1. Catalyst testing

Fig. 1 shows the evolution of CH_4 and CO_2 conversion (XCH_4 and XCO_2, respectively) and H_2/CO relation vs. time. The experiment
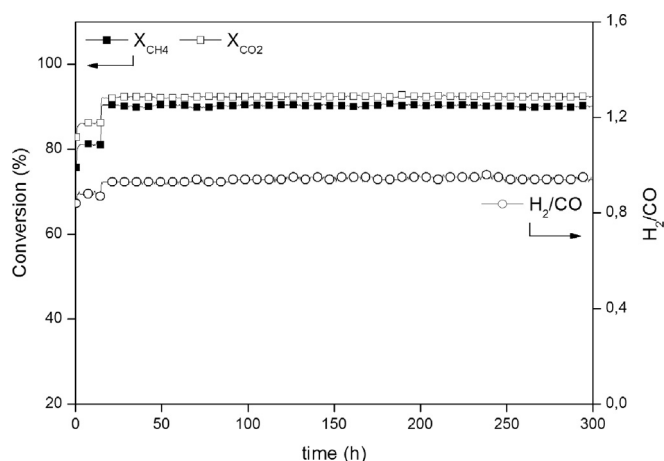

Fig. 1. CH_4 and CO_2 conversion and H_2/CO ratio vs. time in dry reforming of methane. Testing conditions: CO_2:CH_4 = 1750 °C and space velocity equal to 4800 cm^3 g_{cat}^{-1} h^{-1}.

was kept for 300 h, where first 20 h were performed at 700 °C. An initial activation period of 5 h was detected which can be ascribed to the formation of new active sites when the catalyst was exposed to the reaction mixture [11,27].

CO_2 conversion was higher than CH_4 conversion, due to the reverse water–gas-shift reaction (RWGS: $CO_2 + H_2 \leftrightarrows H_2O + CO$) [17]. The presence of H_2O (3%) in the product stream (not shown) and the H_2/CO ratio (0.95) below the theoretical (1) confirmed this fact. Furthermore, both conversions are higher than thermodynamic equilibrium estimation (87%), which suggest that other reactions are taking place. Other possible reactions are methane decomposition ($CH_4 \leftrightarrows H_2 + C$), Boudouard reaction ($2CO \leftrightarrows C + CO_2$) or methane steam reforming ($CH_4 + H_2O \leftrightarrows 3H_2 + CO$) which will consume water formed by means of RWGS reaction [22].

It is remarkable the great stability of the catalyst, not having detected any sign of deactivation during the whole test. Comparing our catalytic test of those mentioned in the Introduction section [23–26], we operated at lower temperature than these reported experiments with exception of Zhang et al. [26]; and without diluting the feeding in the manner of Xu et al. [23], what means that our working conditions facilitates more carbon deposition and therefore, catalyst deactivation. We also operated at a higher space velocity than Kang et al. [24] and Al-Fatesh et al. [25] experiments, which means that our catalyst is more active. Despite these more demanding conditions, our catalyst was stable during a longer period of time.

3.2. Post-reaction characterization

Characterization of the used catalysts was performed in order to evaluate whether carbon was deposited and its nature. The average coking rate was calculated from the weight loss from thermogravimetric results, caused by CO_2 formation, and divided by the duration of the test (300 h). It was 2 mg g_{cat}^{-1} h^{-1}, that is, higher than the rate reported by Xu et al. [23] (0.0946 mg g_{cat}^{-1} h^{-1}) and Al-Fatesh et al. [25] (0.12 mg g_{cat}^{-1} h^{-1}). It is noteworthy that both catalytic tests were performed at higher temperatures. After performing two other tests: 1) at lower reaction temperature (700 °C) [22] and 2) after a higher reduction temperature treatment (750 °C), we have begun to think that the carbon deposition rate of the test reported in this work is overestimated. The carbon deposition rate of the test-1 was also 2 mg g_{cat}^{-1} h^{-1} despite a 2% CH_4 conversion decrease was detected after 200 h [22]. The rate of test-2 was 0.36 mg g_{cat}^{-1} h^{-1} although the catalyst slightly deactivate after 270 h. Consequently, we think that we probably characterized a not well-homogenized sample. Unfortunately, we do not have enough amount of sample to repeat the characterization. Nevertheless, qualitative analysis is possible yet. The deposited carbon was gasified at 620 °C (Fig. 2). Consequently, this carbon can be classified as inactive carbon [28]. Chen et al. [29] related the burning temperatures of carbon with the degree of crystallization of carbon species. According to them, crystalline carbon can be only burnt out at temperatures as high as 700 °C. Consequently, the carbon deposited in our catalyst may be well crystallized.

A more detailed characterization of the used catalyst was performed using several techniques such as XPS and Raman spectroscopy and SEM and TEM microscopy. XPS characterization of the used catalyst was performed in order to analyse C 1s core level spectrum (Fig. 3), which showed a weak signal at 284.6 eV which is associated with adventitious carbon and represents a 9% of the total amount of carbon. Two more signals were registered around 280.1 and 281.0 eV. The first one, with the highest proportion (60%), is assigned to the formation of carbon nanotubes (CNT) and the second one (24%) to the presence of carbon nanofibres (CNF) [30]. Such carbon species grew above the surface with no physical contact with the
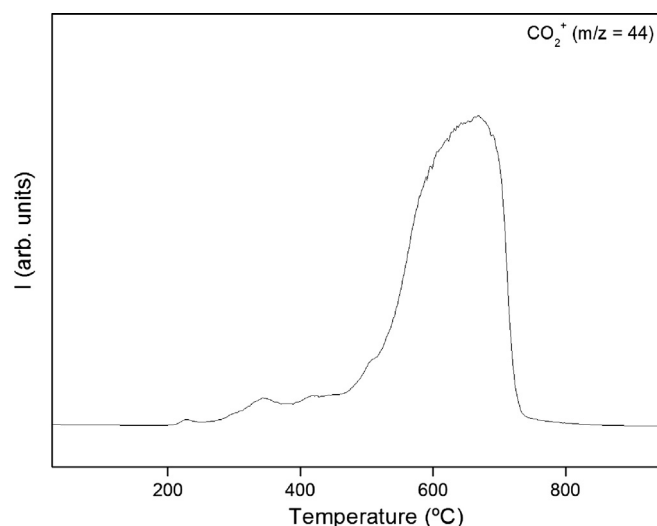

Fig. 2. MS signal (m/z = 44) in TPO characterization experiment for catalyst after test.

catalyst's surface [31]. Another signal was detected at 287.0 eV and may be attributed to superficial carbonates [32].

The Raman spectrum (Fig. 4) displays two main bands D and G at 1350 and 1580 cm^{-1}, the latter with a blue shoulder D′, and two less intense bands 2D (2700 and 2940 cm^{-1}) and G′ (3240 cm^{-1}) [33]. The so-called G-mode is assigned to the in-plane displacement of carbon atoms in the hexagonal sheets. When disorder is introduced into the graphite structure additional bands are found (D, D′ and 2D-modes), which have been assigned to the non-zone-centred phonons associated to the disorder-induced vibration of C–C bond [34–36]. The average I_D/I_G value from five different Raman spectrum spots was 0.7, which indicates the formation of fibres with structural defects [37,38]. The relative intensity ratio, I_D/I_G, can be used to express the graphitization of carbon or the degree of disorder in the structure. This ratio is known to correlate with the in-plane crystal domain size and has been used to estimate the degree of disorder in the graphitic carbon or, conversely, the extent of edge plane graphite [39]. A I_D/I_G ratio near zero indicates high crystallinity (order) and a ratio near to or greater than one demonstrates high disorder due to abundant defects in the graphitic structure. Tan et al. [40] reported values of I_D/I_G = 0.051 for highly oriented
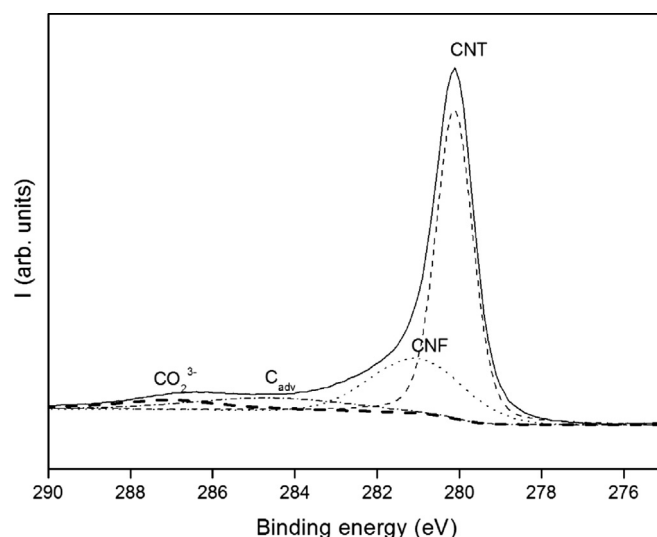

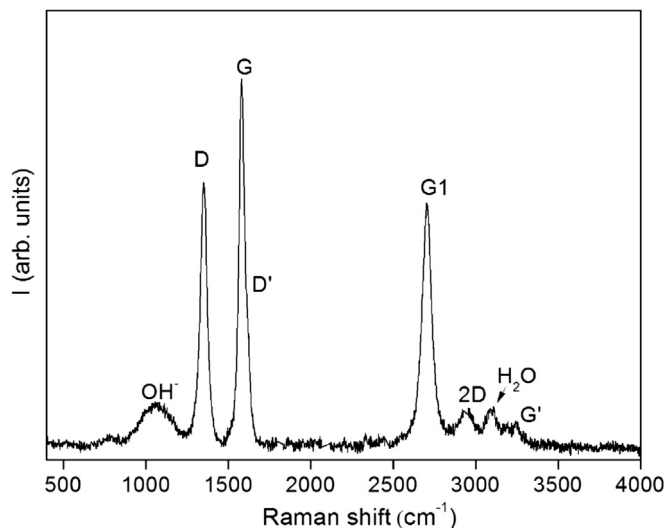**Fig. 3.** C 1s core-level spectra of catalyst after test.

Fig. 4. Raman spectroscopy characterization of used catalyst.

pyrolytic graphite (highly organized), $I_D/I_G = 0.430$ for carbon nanotubes prepared by dc arc discharge and $I_D/I_G = 3.56$ for carbon nanotubes prepared by catalytic methods. Our average I_D/I_G indicates a quite well-crystallization, which agrees with TPO results, although some structural defects may be present.

In addition to the bands ascribed to deposited carbon, other two bands were detected (1054 and 3100 cm^{-1}). First band can be assigned to OH bending vibrations and/or symmetric stretching vibrations of carbonates [41] while second band can be ascribed to stretching water molecules [16].

SEM micrograph (Fig. 5) shows the morphological appearance of the carbon deposited on the still active catalyst after the 300 h test. They consist of curved and nanosized filaments. The growing directions of the fibres are rather random, which may be accounted for the space competition of the growing.

Two different structures were observed in TEM micrographs (Fig. 6). One kind of carbon is hollow nanotubes (Fig. 6b), which consists of carbon platelets aligned parallel to the fibre axis (MWCNT). In agreement with SEM photographs, the fibres are arranged in a random fashion. Most of these filaments exhibited some degree of curvature, probably owing to the unequal diffusion of graphitic carbon through the nickel particles [42]. The second type
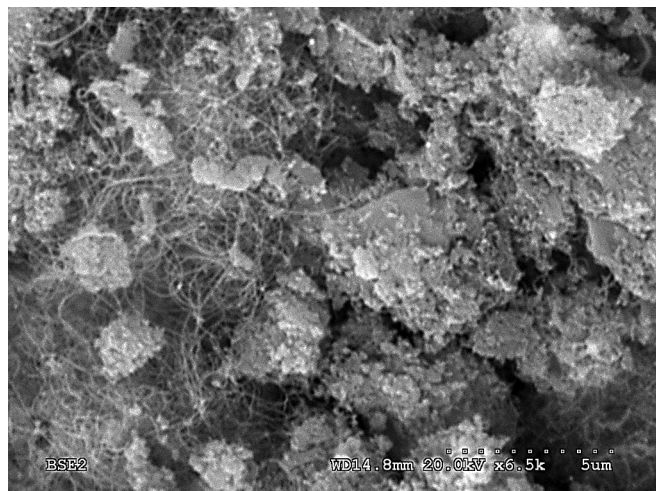

Fig. 5. SEM micrograph of used catalyst.

is graphitic ribbons (Fig. 6c), which consist of platelets aligned parallel to the axis. Both carbons showed a d-spacing along the c axis of 0.340 nm while well-crystallized graphite d-spacing is 0.334 nm, that is, deposited carbon is turbostratic. Apparently, within the growth process, ordering of atoms within a graphene layer is high, but between layers, it is limited [43].

Carbon fibres showed internal partitions formed by the linkage of inner carbon layers. All these internal partitions are oriented perpendicular to the filament axis along one direction. Many defects in the structure was detected, i.e. nano-caps or closed layer structures (Fig. 6b). This leads to the appearance of steps and terraces, formed by the fragments of basal graphite layers. This linkage was bound to happen, since it is thermodynamically favourable. Only a small part of the filament surface is usually represented by open edges of the graphite layers [44]. These results agree with the Raman spectroscopy characterization, which foresee structural defects. The dislocations could be expected to increase the resistivity to fracture upon deformation [45].

It is believed that CH$_4$ decomposition is the initial step of reforming reaction, resulting from the dissociative adsorption of CH$_4$ on the surface of metal particles [26]. Carbon formation occurs when the formation rate of carbon species is higher than its removal rate through its gasification with CO$_2$. It has been concluded that the net formation of carbon on Ni-based catalysts is related to Ni particle size. Kim et al. [46] concluded that a minimum diameter about 7 nm is required for the Ni particles to generate filamentous carbon, while Tang et al. [47] settled that the critical size of Ni particle to prevent the formation of tubular whisker carbon is about 10 nm for CO$_2$ reforming of methane. The size distribution of Ni particles in our catalyst, which is the result of the measurement of 169 particles, is presented in Fig. 6c. Two maximums were observed, one at 8 nm and another at 14 nm. Larger particles were observed in Fig. 6a but XEDS analysis confirmed that they consisted mainly on Fe contamination that comes from the walls of the reactor. The broad size distribution seems to be beneficial since no sign of deactivation was observed during the catalytic test, which agrees with Alonso et al. [48] and Horváth et al. [49]. They attributed this beneficial effect to stable decomposition of methane and carbon filament formation favoured by large particles, while small particles causes initial methane decomposition. However, they also suggested that if the filamentous carbon formation is accelerated, it would be also detrimental causing catalyst plug in and metal particle destroy [50]. Zhang et al. [26] reported that when particles below and above the critical size coexist, the catalyst could maintain stable in a less activity after the larger particles have completely been disabled by carbon. Some authors have also reported that graphite can favour close contact of coke and metal. It acts as CH$_x$ collector and reduces the time of carbon species residence on the metal surface, what can limit the deactivation process [51,52]. Moreover, the presence of defects on the nanotubes structure confers a higher resistivity to fracture what prevent the encapsulation of active sites. When the catalyst was reduced at 750 °C, the Ni particle size distribution was shifted to higher values (17 nm) and a slight deactivation of the catalyst occurred. This confirmed the great importance of Ni particle diameter on catalytic performance.

The presence of filamentous carbon with Ni on the top could also explain the great stability, however, these species were not observed along the surface of our catalyst, as other authors have reported [35,50,53,54].

Other factors that can increase catalyst stability are catalyst physico-chemical properties. As it was mentioned before, catalysts obtained from hydrotalcite calcination have high surface areas, good dispersion and basic properties. These attributes lead to lower Ni particle sintering and a better CO$_2$ adsorption which accelerates
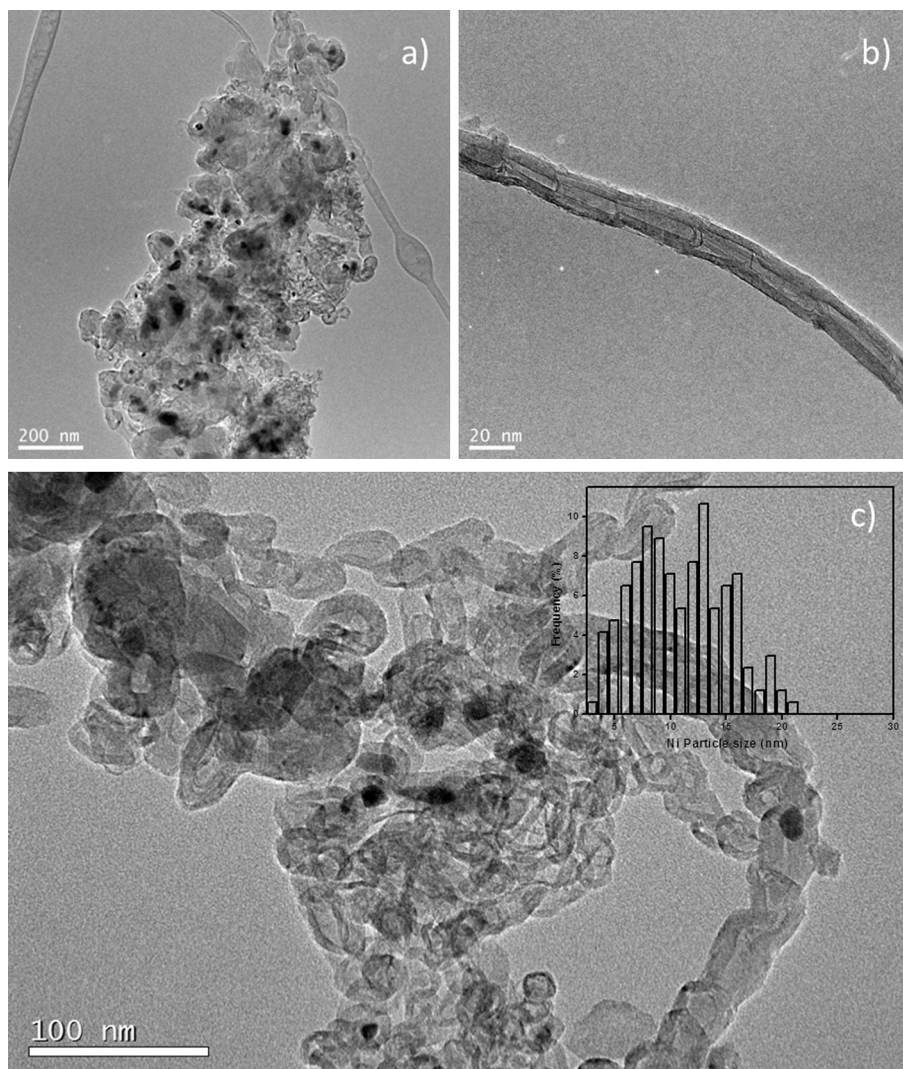
Fig. 6. TEM micrographs of used catalyst: a) general micrograph, b) hollow MWCNT, c) graphitic ribbons and Ni particle size distribution.

the gasification of CH_x species. The addition of lanthanum also increases the adsorption ability of carbon dioxide and improves Ni dispersion [12]. Moreover, $La_2O_2CO_3$ is supposed to be formed in the surface [19] where it helps to gasificate carbon deposits through the reaction $La_2O_2CO_3 + C \leftrightarrows La_2O_3 + 2CO$ [55,56].

4. Conclusions

A long term catalytic test was performed over a La-promoted Ni-based catalyst, obtained from hydrotalcite precursor calcination. The catalyst showed no sign of deactivation during 300 h. CH_4 and CO_2 conversions were higher than thermodynamic equilibrium estimation due to participation of secondary reactions such as Boudouard, CH_4 decomposition, steam reforming or RWGS. This last reaction was also responsible of the higher CO_2 conversion compared with CH_4 conversion.

Characterization of the used catalyst indicated that carbon deposited during the reforming reaction. Two different types of carbon were detected: carbon nanotubes and carbon nanofibres. These filamentous carbon are well-crystallize but they present structural defects such as nanocaps or dislocations, which increases the resistivity to fracture.

The high stability observed during the whole test may indicate that the particles are not encapsulated, allowing the reactants to access them. In addition, graphite can act as a CH_x collector, reducing the time of carbon species residence on the metal surface, what can limit the deactivation process. The presence of defects on the structure of nanotubes confers a higher resistivity to fracture what prevent the encapsulation of active sites. The small Ni particles diameters, together with its broad distribution seem to have a beneficial effect on the catalytic performance. In addition, the good catalytic performance can be also associated with basic properties of the catalyst which increases the adsorption ability of carbon dioxide.

Acknowledgements

References

[1] J.R. Rostrup-Nielsen, Catal. Today 63 (2000) 159–164.
[2] N. Muradov, F. Smith, A. T-Raissi, Int. J. Hydrogen Energy 33 (2008) 2023–2035.
[3] J.R.H. Ross, Catal. Today 100 (2005) 151–158.

[4] J.R. Rostrup-Nielsen, Catalytic Steam Reforming, Springer, Berlin, 1984.
[5] M.C.J. Bradford, M.A. Vannice, Appl. Catal. A 142 (1996) 73−96.
[6] S. Haag, M. burgard, B. Ernst, J. Catal. 252 (2007) 190−204.
[7] J.A.C. Dias, J.M. Assaf, Catal. Today 85 (2003) 59−68.
[8] F. Solymosi, G. Kutsán, A. Erdöhelyi, Catal. Lett. 11 (1991) 149−156.
[9] M.F. Mark, W.F. Maier, J. Catal. 164 (1996) 122−130.
[10] H. Papp, P. -Schuler, Q. Zhang, Top. Catal. 3 (1996) 299−311.
[11] J.R. Rostrup-Nielsen, J.H.B. Hansen, J. Catal. 144 (1993) 38−49.
[12] M. Benito, S. García, P. Ferreira-Aparicio, L. García Serrano, L. Daza, J. Power Sources 169 (2007) 177−183.
[13] M.C.J. Bradford, M.A. Vannice, Catal. Rev. Sci. Eng. 41 (1999) 1−42.
[14] E. Ruckenstein, Y.H. Hu, Appl. Catal. A 133 (1995) 149−161.
[15] A. Bhattacharyya, V.W. Chang, D.J. Schumacher, Appl. Clay Sci. 13 (1998) 317−328.
[16] F. Cavani, F. Trifirò, A. Vaccari, Catal. Today 11 (1991) 173−301.
[17] A. Serrano-Lotina, L. Rodríguez, G. Muñoz, L. Daza, J. Power Sources 196 (2011) 4404−4410.
[18] J.Z. Luo, Z.L. Yu, C.F. Ng, C.T. Au, J. Catal. 194 (2000) 198.
[19] X.E. Verykios, Int. J. Hydrogen Energy 28 (2003) 1045.
[20] A. Serrano-Lotina, A.J. Martin, M.A. Folgado, L. Daza, Int. J. Hydrogen Energy 37 (2012) 12342−12350.
[21] A. Serrano-Lotina, L. Rodríguez, G. Muñoz, A.J. Martin, M.A. Folgado, L. Daza, Catal. Commun. 12 (2011) 961−967.
[22] A. Serrano-Lotina, Obtención de hidrógeno a partir de biogas mediante catalizadores derivados de hidrotalcita. PhD Thesis, Univ. Autónoma de Madrid, 2012.
[23] J. Xu, W. Zhou, Z. Li, J. Wang, J. Ma, Int. J. Hydrogen Energy 34 (2009) 6646−6654.
[24] K.-M. Kang, H.-W. Kim, I.-W. Shim, H.-Y. Kwak, Fuel Proc. Tech. 92 (2011) 1236−1243.
[25] A.S.A. Al-Fatesh, A.H. Fakeeha, A.E. Abasaeed, Chin. J. Catal. 32 (2011) 1604−1609.
[26] J. Zhang, H. Wang, A.K. Dalai, Appl. Catal. A 339 (2008) 121−129.
[27] Z. Zhang, X.E. Verykios, App. Catal. A 138 (1996) 109−133.
[28] J. Guo, H. Lou, X. Zheng, Carbon 45 (2007) 1314−1321.
[29] L. Chen, Y. Lu, Q. Hong, J. Lin, F.M. Dautzenberg, Appl. Catal. A 292 (2005) 295−304.
[30] M. García-Diéguez, C. Herrera, M.A. Larrubia, L.J. Alemany, Catal. Today 197 (2012) 50−57.
[31] B. Pawelec, S. Damyanova, K. Arishtirova, J.L.G. Fierro, L. Petrov, Appl. Catal. A 323 (2007) 188−201.
[32] M. García-Diéguez, I.S. Pieta, M.C. Herrera, M.A. Larrubia, L.J. Alemany, J. Catal. 270 (2010) 136−145.
[33] F. Tuinstra, J.L. Koenig, J. Chem. Phys. 53 (1970) 1126−1131.
[34] A.L. Pinheiro, A.N. Pinheiro, A. Valentini, J.M. Filho, F.F. Sousa, J.R. Sousa, M.G.C. Rocha, P. Bargiela, A.C. Oliveira, Catal. Commun. 11 (2009) 11−14.
[35] F.F. Sousa, H.S.A. Sousa, A.C. Oliveira, M.C.C. Junior, A.P. Ayala, E.B. Barrosa, B.C. Viana, J.M. Filho, A.C. Oliveira, Int. J. Hydrogen Energy 37 (2012) 3201−3212.
[36] M.J. Matthews, M.A. Pimenta, G. Dresselhaus, M.S. Dresselhaus, M. Endo, Phys. Rev. B 59 (1999) 6585−6588.
[37] L. Zhang, F. Li, X. Xiang, M. Wei, D.G. Evans, Chem. Eng. J. 155 (2009) 474−482.
[38] H. Özdemir, M.A.F. Óksüzömer, M.A. Gürkaynak, Int. J. Hydrogen Energy 35 (2010) 12147−12160.
[39] D. Geng, Y. Cheng, Y. Chen, Y. Li, R. Li, X. Sun, S. Ye, S. Knight, Energy Environ. Sci. 4 (2011) 760−764.
[40] P. Tan, S. Zhang, K. To Yue, F. Huang, J. Raman Spectrosc. 28 (1997) 369−372.
[41] J. Pérez-ramírez, G. Mul, J.A. Moulijn, Vib. Spectrosc. 27 (2001) 75−88.
[42] S. Natesakhawat, R.B. Watson, X.Q. Wang, U.S. Ozkan, J. Catal. 234 (2005) 496−508.
[43] K.P. Jong, J.W. Geus, Catal. Rev. Sci. Eng. 42 (2000) 481−510.
[44] T.V. Reshetenko, L.B. Avdeeva, Z.R. Ismagilov, V.V. Pushkarev, S.V. Cherepanova, A.L. Chuvilin, V.A. Likholobov, Carbon 41 (2003) 1605−1615.
[45] Y. Li, J. Chen, L. Chang, Appl. Catal. A 163 (1997) 45−57.
[46] J.-H. Kim, D.J. Suh, T.-J. Park, K.-L. Kim, Appl. Catal. 197 (2000) 191−200.
[47] S. Tang, L. Ji, J. Lin, H.C. Zeng, K.L. Tan, K. Li, J. Catal. 194 (2000) 424−430.
[48] D. San-José-Alonso, J. Juan-Juan, M.J. Illán-Gómez, M.C. Román-Martínez, Appl. Catal. A 371 (2009) 54−59.
[49] A. Horváth, G. Stefler, O. Gestzi, A. Kienneman, A. Pietraszek, L. Guczi, Catal. Today 169 (2011) 102−111.
[50] F. Pompeo, N.N. Nichio, O.A. Ferretti, D. Resasco, Int. J. Hydrogen Energy 30 (2005) 1399−1405.
[51] P. Ferreira-Aparicio, C. Marquez-Álvarez, I. Rodríguez-Ramos, Y. Schuurman, A. Guerrero-Ruiz, C. Mirodatos, J. Catal. 184 (1999) 202−212.
[52] C. Gennequin, M. Safariamin, S. Siffert, A. Aboukaïs, E. Abi-Aad, Catal. Today 176 (2011) 139−143.
[53] Y. Qu, A.M. Sutherland, T. Guo, Energy Fuels 22 (2008) 2183−2187.
[54] M.H. Amin, K. Mantri, J. Newnham, J. Tardio, S.K. Bhargava, Appl. Catal. B 119−120 (2012) 217−226.
[55] V.A. Tsipouriari, X.E. Verykios, J. Catal. 187 (1999) 85−94.
[56] A.N. Fatsikostas, D.I. Kondarides, X.E. Verykios, Catal. Today 75 (2002) 145−155.